Development of a Power Efficient, Restartable, "Green" Propellant Thruster for Small Spacecraft and Satellites

Stephen A. Whitmore, Stephen L. Merkley, Zachary S. Spurrier, Sean D. Walker
Mechanical and Aerospace Engineering Department, Utah State University
4130 Old Main Hill, UMC 4130; (435)-797-2951
Stephen.Whitmore@usu.edu

This paper details the design, developmental, and testing of an innovative, flight-weight, "green" hybrid propulsion system of a size that is applicable to a wide range of small spacecraft missions. The system uses environmentally friendly compressed gaseous oxygen and ABS-plastic as propellants, and is designed as a "drop in" replacement for monopropellant hydrazine spacecraft propulsion systems. The design leverages robotic manufacturing (RM) to build the fuel grain and other system components including the nozzle, motor case, and injector cap. The inherently safe design well-suited for rideshare missions. Test results from a medium scale laboratory weight motor and a small flight weight thruster are presented. The achieved laboratory specific impulse exceeds 230 seconds, and this value extrapolates to greater than 300 seconds under spaceflight conditions -- significantly higher than can be achieved by hydrazine-based systems. A small 22-N thruster has been successfully design and built. Preliminary tests have shown capability to perform multiple restarts with very little startup latency.

I. Introduction

A recent study by the European Space Agency Space Research and Technology Center (*ESTEC*) has identified two essential design elements to achieving low cost commercial space access and operations; *1) Reduced production, operational, and transport costs due to lower propellant toxicity and explosion hazards,* and *2) Reduced costs due to an overall reduction in subsystems complexity and overall systems interface complexity.* [1], [2] The *ESA/ESTEC* study showed the potential for considerable operational cost savings by simplifying propellant ground handing procedures. Developing a non-toxic, stable “green” alternative for the most commonly used in-space propellant - hydrazine - was highly recommended. [3]

Although procedures are in place to allow hydrazine to be managed safely on tightly controlled military reservations and at government-operated launch facilities; the toxicity and explosion potential of hydrazine requires extreme handling precautions that increase operational complexity. Increasingly, with a growing regulatory burden, infrastructure requirements associated with hydrazine transport, storage, servicing, and clean-up of accidental releases are becoming cost prohibitive. As space flight operations continue to shift from government–run organizations to privately-funded ventures operating off-site from government-owned test reservations, servicing payloads requiring hydrazine as a propellant becomes operationally infeasible.

Extreme handling precautions generally do not favor hydrazine as a propellant for secondary payloads. Secondary payloads that rely on toxic or hazardous propellants, and present a significant risk to the primary payload, are currently excluded under most launch rules. Thus, because the vast majority of small commercial spacecraft rely on "rideshare" or secondary payload launch opportunities, development of a safe, clean, and replacement for hydrazine-based propulsion systems is especially critical for the emerging commercial space industry.

A useful "green" replacement for hydrazine must be sufficiently chemically and thermally stable to allow technicians and engineers to safely work with the propellant in normal "shirt-sleeve" commercial environment; but must reliably combust and have good performance properties. Cryogenic or high freezing point propellants requiring temperature control are not appropriate for space propulsion applications. Although mass-specific impulse is important, volume-specific impulse *(density impulse)* is an even more important consideration, and a high propellant storage density is preferred.

For the past decade the US Air Force (USAF) and the Swedish Space Corporation (SSC) subsidiary *Ecological Advanced Propulsion Systems* (ECAPS) have been pursuing green-propellant alternatives based on aqueous solutions of *ionic liquids*. Ionic liquids are water-soluble ammonium-salts that normally exist in solid form at room temperature, but melt below the boiling point of water. These types of propellants give technicians the ability to work in a more relaxed environment due to the less-toxic nature of the propellants, however, there exist several key developmental issues associated with IL-based propellants that make them unsuitable for small spacecraft applications. The current technique in igniting these propellants use an energy-hungry and cost-inhibitive catalyst beds that are infeasible to use in small spacecraft with limited power. Also, due to very slow reaction kinetics [4] at moderate pressures (2000-3000 kPa) system latencies associated with IL-based propellants are significant for moderate chamber pressures and may limit the usefulness of IL-propellants for reaction control systems.

Clearly, significant technology improvements must occur before IL-based systems can be employed as a primary propulsion unit or as part of the reaction control system for small spacecraft. With the current state of propulsion technology, the only proven non-hazardous propulsion alternative to hydrazine, and available for small ride-share payloads, is based on low-performing cold-gas thrusters.

II. HYBRID ROCKET SYSTEMS AS A "GREEN" SPACE PROPULSION ALTERNATIVES

When compared to conventional liquid-and solid-propelled rocket systems, hybrid rockets -- where the propellants typically consist of a benign liquid or gaseous oxidizer and an inert solid fuel -- possess well-known operational safety and handling-advantages. A study by the U.S. Department of Transportation concluded that hybrid rocket motors can be safely stored and operated without a significant risk of explosion or detonation, and offer the potential to significantly reduce operating costs for commercial launch vehicles. [5] Hybrid rocket systems offer higher performance than hydrazine-based systems; and their inherent-design safety offers a significant potential for ride-share spacecraft applications. However, in spite of these well-known safety and handling advantages; conventionally-designed hybrid rocket systems have not seen widespread commercial use due to several key drawbacks that exist with conventional hybrid-system designs.

A. Disadvantages with the Current State-of-the-Art in Hybrid Rocket System

First, the internal motor ballistics of hybrid combustion produce fuel regression rates typically 25-30% lower than solid fuel motors in the same thrust and impulse class. [6] These lowered fuel regression rates tend to produce unacceptably high oxidizer-to-fuel (O/F) ratios that lead to combustion instability, erosive burning, nozzle erosion, and reduced motor duty cycles. To achieve O/F ratios that produce acceptable combustion characteristics, traditional cylindrical fuel ports have been fabricated with very long length-to-diameter ratios. This high aspect ratio results in poor volumetric efficiency that is incompatible with small spacecraft applications.

Second, because of the relative propellant stability, hybrid rocket systems can be difficult to ignite; and a substantial ignition enthalpy source is required. The ignition source must provide sufficient heat to pyrolize the solid fuel grain at the head end of the motor, while simultaneously providing sufficient residual energy to overcome the activation energy of the propellants. Such high-energy devices often come with a suite of environmental and objectives risks, and operational challenges.

Most conventional hybrid rocket applications have used high output pyrotechnic or “squib” charges to initiate combustion. Pyrotechnic charges are extremely susceptible to the Hazards of Electromagnetic Radiation to Ordnance (HERO) [7], and large pyrotechnic charges present a significant explosion hazard that is incompatible with rideshare opportunities. Most importantly, for nearly all applications pyrotechnic ignitors are designed as "one-shot" devices that do not allow a multiple restart capability. Thus the great potential for re-startable upper stages or in-space maneuvering systems using hybrid propulsion remains largely unrealized. An operational hybrid system with multiple restart capability does not currently exist.

Finally, the "cast and cure" methods for producing conventional thermosetting hybrid fuel grain materials including Hydroxyl-Terminated Polybutadiene (*HTPB*), Polybutadiene Acrylonitrile (*PBAN*), and Glycidyl Azide Polymer (*GAP*) are necessarily labor intensive, and high production rates cannot be achieved without a significant manufacturing infrastructure. These binder materials are mixed from liquid base-components, degassed under vacuum, and then cast and cured in a fuel grain mold. This labor intensive manufacture and assembly approach results in market prohibitive production costs and cannot produce the numbers, varieties of motors, and consistency of manufacturing between each motor required to support the what is expected to be a fast-growing commercial space industry.

The isocyanate-based materials used to cure these previously described fuel polymers present a wide variety of Environmental Safety and Occupational Health (ESOH) risks including carcinogenic and detrimental reproductive effects. The US Department of Defense considers these materials to be environmentally unsustainable for large-scale propellant production, and is actively seeking replacement alternatives. [8]

B. Additive Manufacturing as a Solution to Existing Hybrid Propulsion Technology Disadvantages

Whitmore and Peterson at Utah State University, have recently investigated the use of additively-manufactured Acrylonitrile Butadiene Styrene (ABS) thermoplastic as a hybrid rocket fuel material. A key was outcome of this research was the demonstrated thermodynamic equivalence of ABS to the conventional hybrid rocket fuel hydroxyl-terminated polybutadiene (HTPB) when burned with nitrous oxide (N_2O). ABS achieved specific impulse (I_{sp}) and characteristic velocity (c^*) that are nearly identical to HTPB. ABS and HTPB fuel regression massflow rates for cylindrical fuel ports were measured to be nearly identical.

When compared to HTPB, however, ABS has several mechanical properties that make it very attractive as a hybrid rocket fuel. ABS is an inexpensive thermoplastic material that is widely mass-produced for a variety of non-combustion applications including household plumbing and structural materials. ABS is a non-crystalline material with an amorphous structure. As such ABS does not possess a true melting point, but exists in a highly "softened" semi-fluid state before vaporizing. This fluid state exists over a wide temperature range.

1) Additive Manufacturing of Hybrid Propellants

This melting property makes ABS the material of choice for a modern form of additive manufacturing known as Fused Deposition Modeling (FDM). In FDM, a plastic filament is unwound from a coil and supplies material to an extrusion nozzle. The nozzle is heated to melt the material and can move in both the horizontal and vertical directions by a computer numerically controlled (CNC) mechanism. Exploiting the FDM fabrication process for ABS offers the potential to revolutionize the manufacture of hybrid rocket fuel grains. FDM can support high production rates and offers the potential of improving hybrid fuel grain quality, consistency, and performance, while reducing development and production costs. These manufacturing advantages cannot be achieved using the conventional methods of solid propellant production. Identical pieces can be produced simultaneously by multiple vendors using a well-developed commercial technology.

2) Arc-Ignition of FDM-Processed ABS Fuel Grains

Finally, FDM-processed ABS possesses unique electrical breakdown properties that can be exploited to allow for rapid on-demand system ignition. Even though the ABS material possesses a very high electrical resistivity and dielectric strength and is not normally considered to be an electrical conductor, [22] as FDM-processed ABS is subjected to a moderate electrostatic potential field the layered material structure concentrates minute electrical charges that produce localized arcing between material layers. Joule heating from the resulting arc produces a small but highly-conductive melt layer. This melt layer allows for very strong surface arcing to occur at moderate input voltage levels (between 200 and 300 Volts). Additional Joule heating from the strong surface arcing causes a sufficient amount of fuel material to be vaporized to seed combustion when simultaneously combined with an oxidizing flow.

The discovery of ABS' unique electrical breakdown characteristics prompted the invention of an ignition system that takes advantage of the previously described "hydrocarbon seeding" phenomenon. Figure 1 illustrates the current iteration of the development of an additively-manufactured ignitor, which is fully-integrated in an ABS fuel grain segment. It is thought that the layered structure of the FDM-processed ABS provides local surface features of very small radius, and it's effect is to produce a large collection of "electrodes" with a gap-distance on the order of fractions of a millimeter. The following image shows the electrostatic arc as it moves along the fuel grain surface. Pyrolyzed gas can also be observed burning in the ambient oxygen.

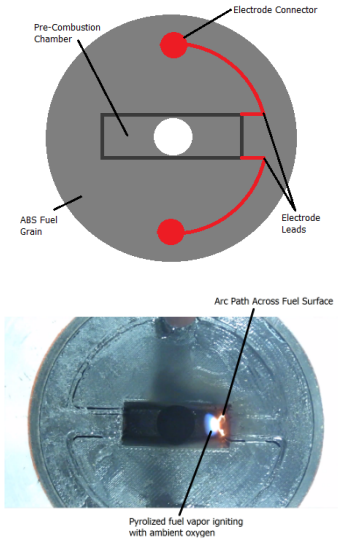

Figure 1. Arc Ignitor Joule-Heating Concept Illustration and Demonstration.

III. System Prototype Test Results

A. Embedded Arc-Ignitor Development and Testing

A series of incremental developmental tests were performed in or to determine the most appropriate geometry for the arc-ignition fuel grain. Reference 14 describes these developmental experiments in detail. Two fundamental generations of prototypes were built and tested. The first generation ignition system was designed as an external "strap-on" ignitor. The strap on ignitor replaced the pyrotechnic charges that were previously used for the motor ignition system. The second-generation system reconfigured the strap-on ignitor to move the system inside of the combustion chamber with the ignitor fuel grain section an integral part of the main motor fuel grain.

Figure 2 presents representative test results from the embedded ignitor grain configuration tests. For these tests gaseous oxygen (GOX) and ABS were used as the propellants. Here the thrust, chamber pressure, ignition current, and thruster input/output power time histories are plotted for multiple motor burns. As can be observed, the chamber pressure rises rapidly once a level of approximately 28 psia is achieved, indicating combustion. This pressure represents a minimum oxygen concentration required for ABS combustion. At the highest injector inlet pressures (and the resulting chamber pressures) the ignition latencies diminish to less than 10 msec.

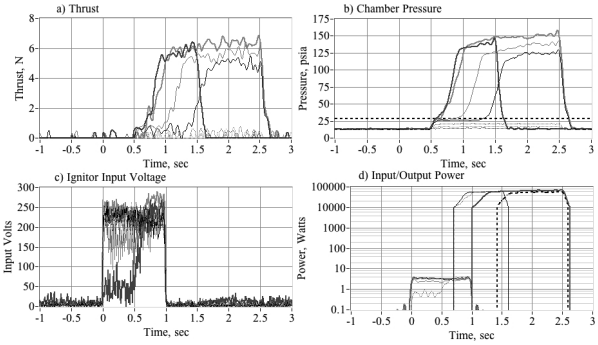

Figure 2. Dual-shelf Ignitor, Co-Axial Injector Test Results.

It can be observed that the input power required for ignition is very small -- less than 4 watts -- whereas, whereas the generated power exceeds *60 Kilowatts. Thus the ignitor system produces a power amplification factor of greater than 15,000!*

B. Integrated Motor Testing

The GOX/ABS ignition tests were concluded by embedding a scaled version of the imbedded ignitor into the top end of a lab scale 75 mm, 170 N thrust hybrid rocket motor. Figure 3 shows the motor layout with the integrated ignitor section and the helical fuel port. The integration of the ignitor into the fuel grain reduced the complexity of the rocket assembly process, and allows the spark ignitron to re-ignite the fuel as long as fuel remains in the ignitor section. The pictured motor configuration of figure 3 shows an embedded helical structure designed to increase regression rate and combustion efficiency. The design takes advantage of FDM-processing to build the ABS ignitor and fuel grain sections with "snap-together" interlocks that allow individual grain segments to be manufactured separately and then assembled for combustion.

After performing various “hands-off” tests, it was found that the response fidelity of the integrated system is consistently greater than was obtained with the initial low chamber volume test apparatus, indicating that the additional chamber volume downstream of the ignitor section has little effect upon the ignition kinetics.

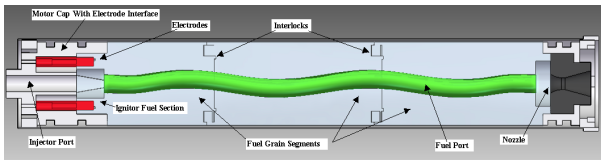

Figure 3. Hybrid Motor with Integrated Ignitor and Interlocking Fuel Grain Segments.

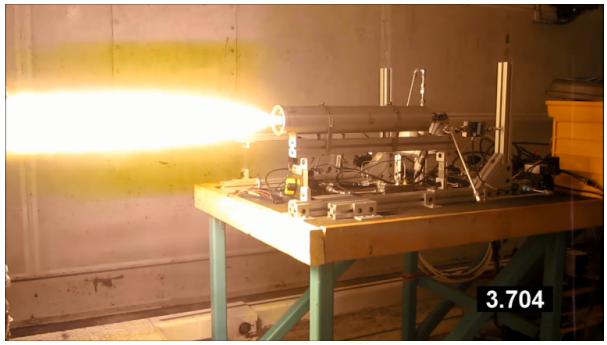

Figure 4. Hybrid Motor Ignition.

For these tests, the motor featured a semi-optimized nozzle with an expansion ratio of 3.5. The mean delivered I_{sp} at ambient conditions was 228.7 seconds. This delivered specific impulse extrapolates to a vacuum I_{sp} of greater than 300 seconds using a 20:1 expansion ratio nozzle -- significantly higher than can be achieved by a hydrazine-based system.

C. Regression Rate Enhancement with Helical Port Structures

Using additive manufacturing hybrid fuel grains can be fabricated with an almost infinite range of fuel port shapes, allowing for significant enhancement of burn properties and combustion efficiencies. Of particular interest are helical fuel structures. It is well known that helical pipe flows have the effect of significantly increasing the local skin friction coefficient. Helical flows also introduce a centrifugal component into the flow field. In hybrid rocket applications, this centrifugal component has the effect of thinning the wall boundary layer, bringing the flame zone closer to the wall surface and increasing the flame diffusion efficiency. [9]

The helical structure is defined by three parameters, 1) the nominal fuel port diameter D_0, the helix loop diameter d, and the helix pitch length, P. The pitch length is defined as the distance between the centerlines of two consecutive helical wraps. The helical *pitch ratio* is defined as the two times the radius of curvature divided by the initial port diameter. In order to model the regression rate amplification of a helical port structure, two factors have to be taken into consideration; 1) an increase in skin friction imparted to the walls of the fuel port, and 2) centrifugal force applied to the fuel port wall that suppresses the regression-rate-“wall blowing” effect resulting from the pyrolyzed fuel emanating from the fuel grain surface.

1) Skin Friction Model

It is well known that helical pipe flows exhibit significantly greater surface skin friction coefficients. For this analysis the skin friction enhancement due to the helical flow pattern is based on a correlation previously developed my Mishra and Gupta. [11]. This model was modified to take into account the diminishing helical radius of curvature as the fuel port burns, resulting in a more cylindrical fuel grain as the burn progresses.

$$C_{f_{helix}} = C_{f_{straight}} + 0.0075 \cdot \sqrt{\frac{D}{2 \cdot R_c}} \tag{1}$$

where $C_{f\,helix}$ is the skin friction coefficient for the helical coil, $C_{f\,straight}$ is the skin friction coefficient for a straight tube, and D is the instantaneous fuel port diameter. The *radius of curvature* of the helical arc is calculated from the loop diameter (d) and pitch length (P) as

$$R_c = \frac{d}{2} \cdot \left(1 + \left(\frac{P}{\pi \cdot r} d \right)^2 \right) \tag{2}$$

The amplification factor due to this effect is calculated as the ratio of the difference of the straight port coefficient of friction to the helical port coefficient. This coefficient is calculated instantaneously throughout the burn based on the changing diameter of the fuel port.

$$A_{Cf} = \frac{C_{f_{straight}} + 0.0075 \cdot \sqrt{\frac{D}{2 \cdot R_{c_{eff}}}}}{C_{f_{straight}}} = 1 + \frac{0.0075}{C_{f_{straight}}} \cdot \sqrt{\frac{D}{2 \cdot R_c \cdot \sqrt{\left(1 + \frac{\pi}{2} \cdot \left(\frac{D - D_{o)}}{R_c} \right)^2 \right)}}} \tag{3}$$

R_{ceff} is the effective helical port radius of curvature given by

$$R_{c_{effective}} = R_c \cdot \sqrt{\left(1 + 2\pi \cdot \left(\frac{s}{R_c} \right)^2 \right)} = R_c \cdot \sqrt{\left(1 + \frac{\pi}{2} \cdot \left(\frac{D - D_{o)}}{R_c} \right)^2 \right)} \tag{4}$$

D_0 is the initial fuel port diameter, and R_c is the radius of the curvature of the initial fuel port centerline.

2) Radial Blowing Suppression Model

In any hybrid, as the fuel burns off the grain surface, it pushes the boundary layer outward toward the center of the port flow, reducing the effectiveness of the boundary layer mixing process and insulating the convective heat transfer zone from the fuel grain surface. Figure 5 illustrates this concept. It is this radial "wall blowing" that is the primary cause for the low fuel regression rates typically observed in hybrid fuel combustion. As mentioned earlier, the helical fuel port induces a centrifugal component of the flow that pushes the flame zone closer to the burning fuel grain surface.

As an approximation of this process Boardman [12] modifies Lees' [13] model of radial emanating flow as

$$C_f = C_{f_0} \frac{1.27}{\beta^{0.77}} \tag{4}$$

$$\beta = \left(\frac{\rho_{wall} \cdot V_{wall}}{\rho_{ox} \cdot V_{ox} \cdot S_t} \right) \approx \frac{\Delta h_{surface}}{h_v} \tag{5}$$

where β is Lees' "blowing coefficient" approximated as the convective heat transfer from the flame zone to the fuel surface divided by the enthalpy of vaporization of the fuel.

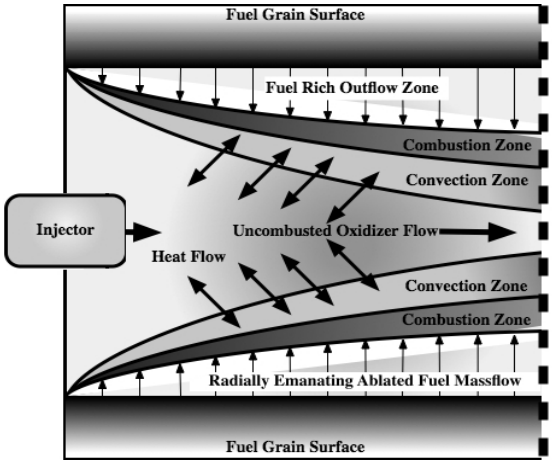

Figure 5. Hybrid Fuel Regression Rate Enthalpy Balance Model.

Using this ratio in an empirical model, the resulting semi-analytical blowing suppression amplification factor can be represented as

$$A_\beta = \left(1 + \frac{d / D}{\Delta h_{flame} / h_v} \right)^{0.77} \tag{6}$$

where d is the helical loop diameter, and D is the instantaneous fuel port diameter.

3) Collected Regression Rate Model

For hybrid rockets using helical fuel ports, the enhanced regression rates leads to the ablating fuel contributing significantly to the total port massflux, and must be accounted for in the calculation of skin friction coefficient. Whitmore et al [14] at Utah State University developed the linear regression rate model of Eq. 7 for a cylindrical bore fuel port.

$$\dot{r} = \left(\frac{0.635 \cdot G_{ox}}{P_r^{\frac{2}{3}} \cdot \rho_{\text{fuel}}} \right) \cdot \left(\frac{\Delta h_{\text{surface}}}{h_v} \right) \cdot \frac{C_{f_0}}{\beta^{0.77}} \cdot \left(1 + \frac{2 \cdot r / D}{\Delta h_{flame} / h_v} \right)^{0.77} \tag{7}$$

In Eq. (7) P_r is the Prandtl number, ρ_{fuel} is the density of the fuel, μ is the viscosity of the flow, G_{ox} is the

oxidizer mass flow per unit cross sectional area of the fuel port, and L is the fuel port length.

To model both the skin friction and blowing suppression amplification using Eq. (7), the enhanced regression rate model can be simply represented as

$$\frac{\dot{r}_{helix}}{\dot{r}_{straight}} = A_{\beta} \times A_{Cf} \tag{8}$$

Regression rate amplification factors exceeding 3.0 are predicted by this semi-analytical models.

D. Helical Grain Motor Tests

To verify these predicted regression rate amplification factors, a series of tests were performed using different helical port structures to enhance the fuel regression rates. A series of tests were performed to evaluate the effectiveness of helical fuel port structures in increasing the fuel regression rate. For this series of tests the motor configuration of Figure 3 was used, and the tested fuel grains were manufactured simultaneously as interlocking segments on a Stratasys Dimension® 1200es 3-D FDM printer [10] from standard density ($0.975\ g/cm^3$) ABS stock material. Joints were bonded using commercial grade ABS pipe joint cement.

Four fuel grain geometries, a straight bore-cylindrical grain and three helical ports with varying helix geometries, were tested. Table 1 summarizes the parameters of these fuel grains. Although real time thrust-stand oxidizer massflow and motor mass measurements were obtained; for this testing campaign each grain was burned multiple times, and the motor disassembled after each test to allow intermediate mass measurements as a check on the accuracy of the real-time measurements. In all 24 static firings were performed as a part of this testing campaign.

TABLE 1. FUEL GRAIN GEOMETRIES FOR HELIX REGRESSION TESTS.

Grain No.	**Fuel Port Parameters**				
	Port length, cm (L)	Initial port diameter, cm (D_0)	Initial helix diameter, cm (d)	No. of Fuel Grain Burns	Initial Pitch Ratio, (R_c/D_0)
1	35.98	2.026	---	3	---
2	35.98	1.524	0.762	5	10.382
3	35.98	1.524	1.114	6	7.130
3	35.98	1.524	1.524	6	5.567
4	22.86	1.524	1.143	6	0.587

The instantaneous fuel regression rate was calculated by integrating Eq. (9) over time from an initial condition to the current time to find the instantaneous port radius.

$$\dot{\overline{r}} = \frac{\dot{m}_{fuel}}{\rho_{fuel} \cdot 2\pi \cdot \overline{r} \cdot L} \tag{9}$$

$$\overline{r}(t) = \sqrt{r_0^2 + \int_0^t \frac{\dot{m}_{fuel} \cdot dt}{\rho_{fuel} \cdot \pi \cdot L}} \tag{10}$$

In Eqs. (9) and (10) $\dot{m}_{fuel}$ is the fuel massflow and r is the port radius, and L is the length of the fuel port.

Figure 6 plots time histories of thrust, chamber pressure, oxidizer massflow, and fuel massflow of all 24 tests for comparison. All of the helical fuel port grains exhibit a significant increase in the mean regression rate. In these graphs the high massflux rates occur early in the burn sequences where the fuel port is still quite helical, and the resulting centrifugal flow effects push the flame zone closer to the wall. As the port burns and the massflux drops, the helical structures also regress both radially and longitudinally, gradually becoming almost cylindrical in shape. The resulting drop in centrifugal force allows radial blowing due to the pyrolized fuel massflow to push the flame zone away from the wall and the regression rate drops significantly. Figure 7 compares the previously developed helical regression rate model against the measured regression rates. Even though this model is based on semi-empirical, the predicted vales closely match the actual integrated instantaneous regression-rate experimental data. Work continues on developing a fully-analytical model.

As the helical loops progressively burn together with time, and the fuel port becomes more and more like a cylinder. This effect is proportional to the initial burn rate; thus, the short pitch length fuel grain where the helical loops are spaced closely together longitudinally shows the most rapid drop over time in regression rate. Conveniently, this effect reduces the potential for excessive unburned fuel "slivers" at the end of the burn lifetime of the fuel grain.

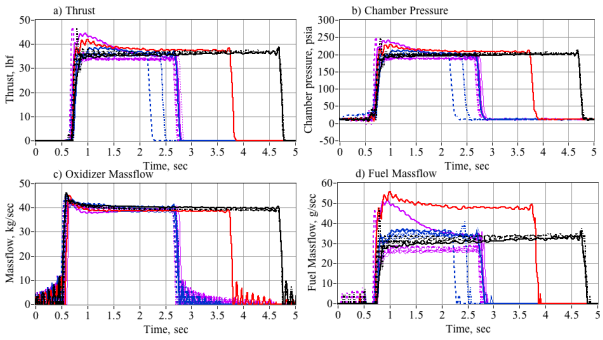

Figure 6. Time histories of all burns (Table 1).

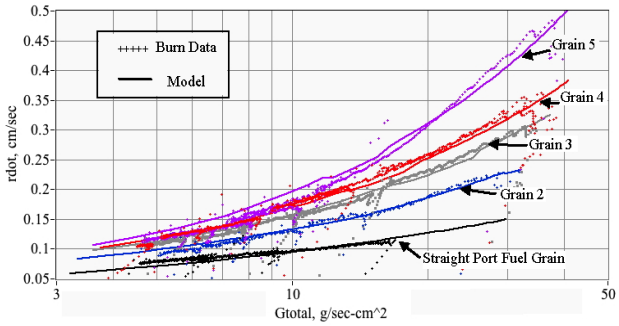

Figure 7. GOX-ABS Regression Rate Data and Model Comparison for Straight-Bore and Helical Grains.

IV. Flight-Weight System Development and Testing

After proof of concept tests with the ignitor, and lab-scale integration tests were completed to prove the simulation models presented in section III, an effort was made to scale down the thruster to semi flight-weight scale to prove the scalability of the system and immediate pulsed re-ignitability of the thruster. The previously presented model was used to design a flight-weight unit with a desired 22-N thrust level. The design was scaled down to fit into a 38mm motor case as seen in figures 8 and 9.

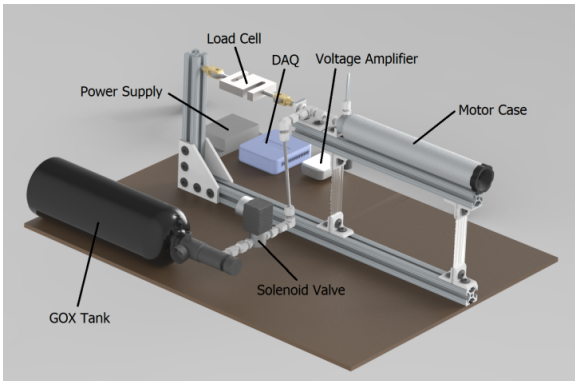

Figure 8. CAD Drawing of Flight-Weight Integrated System

As shown by Figure 9 additive manufacturing was used as before to build the fuel grains for this thruster, utilizing scaled-down electrode leads, closures, and nozzle. Figure 10 shows an example of a chamber pressure time history of a pulsed burn in this new, semi-flight weight, integrated configuration. Figure 11 shows the small thruster firing.

Figure 12 shows the chamber pressure time history trace that was measured as the motor was pulse-fired. As shown, the system was successfully restarted multiple times, with startup transients in the range of ~10msec. Over an ensemble of more than 50 tests, and over a wide range of O/F ratios, the motor was able to ignite and re-ignite with a high level of probability. The only operational limitations of reigniting the motor were during extremely low O/F burn mixtures (O/F < 1). This mode of operation built up carbon soot layers over the spark igniter, thus limiting the amount of fuel vapor permitted to leave the spark path in order to seed combustion. This limitation is of little consequence since in an optimized system, this range of O/F would likely never be observed.

Figure 9.Semi Flight-Weight Integrated System

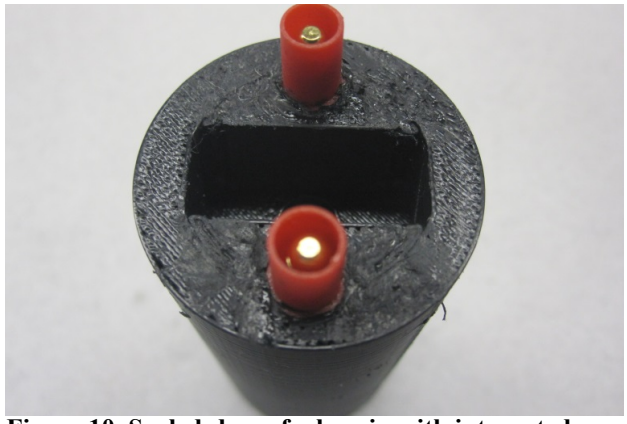

Figure 10. Scaled-down fuel grain with integrated spark ignitor.

The development of this system, along with the results from the previous testing proves the ability of an additively manufactured grain to be used as a "drop-in" replacement for hydrazine, maintaining the consistent restartability and compact form factor of a hydrazine system, while improving significantly on safety, performance, power-consumption, and cost of

materials and operation. Future research will be realized in order to reduce startup transients over wide ranges of chamber pressures and to develop a fully-analytical model of the regression rate amplification factors.

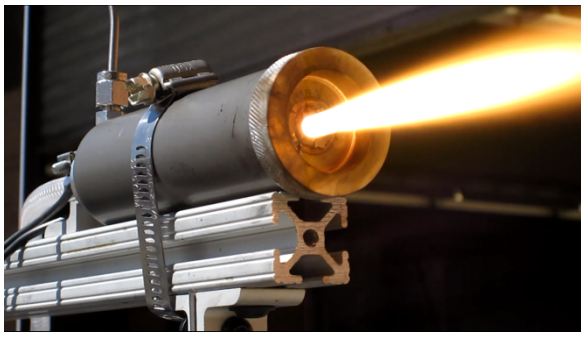

Figure 11. Close-up view of firing thruster

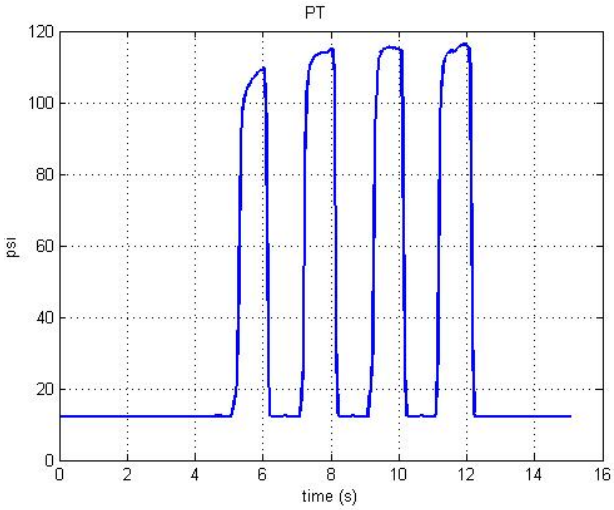

Figure 12. Chamber Pressure Time History of Pulsed Burn (4 burns).

V. CONCLUSION

This paper details the developmental of an innovative low-energy, "green" hybrid propulsion system using Fused Deposition Modeling (FDM) additive manufacturing. When fully developed this cross-cutting technology offers a wide variety of space propulsion applications, and may act as a "drop in" replacement for many existing hydrazine-based propulsion systems. FDM manufacturing circumvents many of the developmental issues normally associated with hybrid rocket systems. FDM manufacturing builds the specimen one layer at a time and produces fuel grain properties that greatly enhance system ignitability and restartabilty. FDM manufacturing has allowed the development of multiple prototype hybrid thrusters that exhibit a high degree of restartability, require a low-wattage input for ignition, demonstrate enhanced fuel regression rates, and offer a highly compact form factor. Presented thruster tests results demonstrate a performance that is superior to hydrazine-based systems in both mass and volumetric specific impulse.

Using additive manufacturing ABS fuel grains can be fabricated with an almost infinite range of fuel port shapes, allowing for significant enhancement of burn properties and combustion efficiencies. Helical ports are found to be most advantageous at enhancing the fuel regression rate. It is well known that helical pipe flows with cylindrical ports show significantly increased end-to-end pressure losses when compared to flows through straight pipes with identical cross sections. Thus, helical flows have the effect of significantly increasing the local skin friction coefficient. Helical flows also introduce a centrifugal component into the flow field. In hybrid rocket applications, this centrifugal component has the effect pushing flame zone closer to the wall surface and increasing the flame diffusion efficiency. In other words, a helical port serves to both increase the surface skin friction coefficient and simultaneous reducing the wall blowing effect, leading to a significant enhancement of the overall regression rate.

This paper summarizes the development of a This paper develops a semi-analytical engineering model to describe the effects of helical fuel ports on hybrid fuel regression rates. The centrifugal flow patterns introduced by the helical fuel port The model decomposes the regression rate amplification factor into two components 1) skin friction enhancement, and 2) wall blowing suppression. The skin friction enhancement due to the helical flow pattern is based on a correlation previously developed by Mishra and Gupta, modified to account for the diminishing helical centerline radius of curvature as the fuel port burns, and the port cross-section becomes increasingly more cylindrical. The radial blowing suppression is modeled as the ratio of the centrifugal force to the rate of momentum flow of the ablated fuel emanating from the port wall. Model predictions are compared to data collected for four different fuel grain geometries using gaseous oxygen and additively-manufactured acrylonitrile butadiene styrene as propellants. The comparisons are quite favorable.

The previously presented model was used to design a flight-weight unit with a desired 22-N thrust level. The small thruster has been successfully fired and has shown capability to perform multiple restarts with very little startup latency. The system was designed to be throttled from a peak thrust of 22 N (5-lbf) to less than 1-N (0.25 lbf) with no loss in performance, stability, and response fidelity. Test results that quantify the minimum reliably achievable impulse-bit as a function of throttle setting and motor duty cycle are currently being performed. A single thruster system with fast-response and stable thrust production across the prescribed 1N-to-22 N range can accomplish a wide variety of space missions including attitude control, reaction wheel de-saturation, and in-orbit maneuvering.

References

[1] Bombelli, V., “Economic Benefits for the Use of Non-toxic Monopropellants for Spacecraft Applications, AIAA-2003-4783, [39th AIAA/ASME/SAE/ASEE Joint Propulsion Conference and Exhibit, Huntsville, AL, July 2003.]

[2] Haeseler, D., Bombelli, V., Vuillermoz, P., Lo, R., Marée, T., & Caramelli, F., “Green Propellant Propulsion Concepts for Space Transportation and Technology Development Needs,” ESA SP-557, [Proceedings of the 2nd International Conference on Green Propellants for Space Propulsion, Cagliari, Sardinia, Italy, 7-8 June 2004.]

[3] Goldstein, Edward, “The Greening of Satellite Propulsion,” Aerospace America, February, 2012, pp. 26-28.

[4] Anon., “Hazard Analysis of Commercial Space Transportation; Vol. 1: Operations, Vol. 2: Hazards, vol. 3: Risk Analysis,” U.S. Dept. of Transportation, PB93-199040, Accession No. 00620693, May 1988.

[5] Katsumi, T., and Hori, K., "Combustion Wave Structure of Hydroxylammonium Nitrate Aqueous Solutions," AIAA 2010-6900, [46th AIAA/ASME/SAE/ASEE Joint Propulsion Conference & Exhibit, 25 - 28 July 2010, Nashville, TN.]

[6] Cheng, C. G., Farmer, R. C., Jones, H. S., and McFarlane, J. S., “Numerical Simulation of the Internal Ballistics of a Hybrid Rocket,” AIAA Paper 94-0554, [30th AIAA/ASME /SAE/ASEE Joint Propulsion Conference & Exhibit, Indianapolis, IN July, 1994.]

[7] Anon., “Department of Defense Interface Standard, Eletromagnetic Environmental Effects requirements for Systems, MIL-STD-464, http:// www.tscm.com/MIL-STD-464.pdf, [Retrieved 8 October 2012].

[8] Anon., "Weapons Systems and Platforms (WP) Focus Area. Environmentally Friendly Sustainable Binder System for Energetic Materials," 2014 Strategic Environmental Research and Development Program (SERDP), Exploratory Development (SEED) BAA-13-0002. This proposal responds specifically to FY2014 SEED Statement of Need, WPSEED-14-01.

[9] Whitmore, Stephen A., Walker Sean D., and Merkley Daniel P., "High Regression Rate Hybrid Rocket Fuel Grains with Helical Port Structures," AIAA-2014-3751, [50th AIAA/ASME/SAE/ASEE Joint Propulsion Conference and Exhibit, Cleveland Medical Mart & Convention Center, Cleveland OH, 28-30 July 2014.]

[10] Anon., "Dimension 1200es, Durability Meets Affordability," http://www.stratasys.com/3d-printers," [Retrieved 25 December 2013.]

[11] Mishra, P., and Gupta, S. N., "Momentum Transfer in Curved Pipes. 1. Newtonian Fluids," J. *Industrial Engineering and Chemical Process Development*, Vol. 18, No. 1, 1979, pp. 130-137.

[12] Sutton, G. P., and Biblarz, O., Rocket Propulsion Elements, John Wiley and Sons, New York, 2001, Appendix 4,5, pp. 731-737.

[13] Lees, L., “Convective Heat Transfer with Mass Addition and Chemical Reactions,” Combustion and Propulsion, 3rd AGARD Colloquium, New York, Pergamon Press, 1958, p. 45.

[14] Whitmore, Stephen A., Walker Sean D., and Merkley, Daniel P., "Engineering Model for Hybrid Rocket Regression Rate Amplification by Helical Fuel Ports," AIAA-2015-2192, 51st AIAA/ASME/SAW/ASEE Joint propulsion Conference, orlando FL 27-29 July 2015.